arXiv:1612.05990v1 [cond-mat.mtrl-sci] 18 Dec 2016

Discovery of a new type of topological Weyl fermion semimetal state in $Mo_xW_{1-x}Te_2$

Ilya Belopolski*,[1] Daniel S. Sanchez*,[1] Yukiaki Ishida*,[2] Xingchen Pan*,[3] Peng Yu*,[4] Su-Yang Xu,[1] Guoqing Chang,[5,6] Tay-Rong Chang,[7] Hao Zheng,[1] Nasser Alidoust,[1] Guang Bian,[1] Madhab Neupane,[8] Shin-Ming Huang,[5,6] Chi-Cheng Lee,[5,6] You Song,[9] Haijun Bu,[3] Guanghou Wang,[3] Shisheng Li,[5,6] Goki Eda,[5,6,10] Horng-Tay Jeng,[7,11] Takeshi Kondo,[2] Hsin Lin,[5,6] Zheng Liu,[4,12,13,†] Fengqi Song,[3,‡] Shik Shin,[2] and M. Zahid Hasan[1,14,§]

[1]*Laboratory for Topological Quantum Matter and Spectroscopy (B7), Department of Physics, Princeton University, Princeton, New Jersey 08544, USA*

[2]*The Institute for Solid State Physics (ISSP), University of Tokyo, Kashiwa-no-ha, Kashiwa, Chiba 277-8581, Japan*

[3]*National Laboratory of Solid State Microstructures, Collaborative Innovation Center of Advanced Microstructures, and Department of Physics, Nanjing University, Nanjing, 210093, P. R. China*

[4]*Centre for Programmable Materials, School of Materials Science and Engineering, Nanyang Technological University, 639798, Singapore*

[5]*Centre for Advanced 2D Materials and Graphene Research Centre, National University of Singapore, 6 Science Drive 2, 117546, Singapore*

[6]*Department of Physics, National University of Singapore, 2 Science Drive 3, 117546, Singapore*

[7]*Department of Physics, National Tsing Hua University, Hsinchu 30013, Taiwan*

[8]*Department of Physics, University of Central Florida, Orlando, FL 32816, USA*

[9]*State Key Laboratory of Coordination Chemistry, School of Chemistry and Chemical Engineering, Collaborative Innovation Center of Advanced Microstructures, Nanjing University, Nanjing, 210093, P. R. China*

[10]*Department of Chemistry, National University of Singapore,*

* These authors contributed equally to this work.

3 Science Drive 3, 117543, Singapore

[11]*Institute of Physics, Academia Sinica, Taipei 11529, Taiwan*

[12]*NOVITAS, Nanoelectronics Centre of Excellence,*
School of Electrical and Electronic Engineering,
Nanyang Technological University, 639798, Singapore

[13]*CINTRA CNRS/NTU/THALES, UMI 3288,*
Research Techno Plaza, 50 Nanyang Drive,
Border X Block, Level 6, 637553, Singapore

[14]*Princeton Institute for Science and Technology of Materials,*
Princeton University, Princeton, New Jersey, 08544, USA

(Dated: December 31, 2016)

Abstract

The recent discovery of a Weyl semimetal in TaAs offers the first Weyl fermion observed in nature and dramatically broadens the classification of topological phases. However, in TaAs it has proven challenging to study the rich transport phenomena arising from emergent Weyl fermions. The series $Mo_xW_{1-x}Te_2$ are inversion-breaking, layered, tunable semimetals already under study as a promising platform for new electronics and recently proposed to host Type II, or strongly Lorentz-violating, Weyl fermions. Here we report the discovery of a Weyl semimetal in $Mo_xW_{1-x}Te_2$ at $x = 25\%$. We use pump-probe angle-resolved photoemission spectroscopy (pump-probe ARPES) to directly observe a topological Fermi arc above the Fermi level, demonstrating a Weyl semimetal. The excellent agreement with calculation suggests that $Mo_xW_{1-x}Te_2$ is the first Type II Weyl semimetal. We also find that certain Weyl points are at the Fermi level, making $Mo_xW_{1-x}Te_2$ a promising platform for transport and optics experiments on Weyl semimetals.

INTRODUCTION

The recent discovery of the first Weyl semimetal in TaAs has opened a new direction of research in condensed matter physics [1–5]. Weyl semimetals are fascinating because they give rise to Weyl fermions as emergent electronic quasiparticles, have an unusual topological classification closely related to the integer quantum Hall effect, and host topological Fermi arc surface states [6–15]. These properties give rise to many unusual transport phenomena, including negative longitudinal magnetoresistance from the chiral anomaly, an anomalous Hall effect, the chiral magnetic effect, non-local transport and novel quantum oscillations [16–18]. Although many recent works have studied transport properties in TaAs [19–21], transport experiments are challenging because TaAs and its isoelectronic cousins have a three-dimensional crystal structure with irrelevant metallic bands and many Weyl points. As a result, there is a need to discover new Weyl semimetals better suited for transport and optics experiments and eventual device applications.

Recently, the $Mo_xW_{1-x}Te_2$ series has been proposed as a new Weyl semimetal [22–25]. Unlike TaAs, $Mo_xW_{1-x}Te_2$ has a layered crystal structure and is rather widely available as large, high-quality single crystals. Indeed, $MoTe_2$, WTe_2 and other transition metal dichalcogenides are already under intense study as a platform for novel electronics [26–30]. Moreover, $Mo_xW_{1-x}Te_2$ offers the possiblity to realize a tunable Weyl semimetal, which may be important for transport measurements and applications. Recently, it was also discovered theoretically that WTe_2 hosts a novel type of strongly Lorentz-violating Weyl fermion, or Type II Weyl fermion, long ignored in quantum field theory [23, 31–38]. This offers a fascinating opportunity to realize in a crystal an emergent particle forbidden as a fundamental particle in particle physics. There are, moreover, unique transport signatures associated with strongly Lorentz-violating Weyl fermions [23, 31–33, 39, 40]. For all these reasons, there is considerable interest in demonstrating that $Mo_xW_{1-x}Te_2$ is a Weyl semimetal. However, it is important to note that *ab initio* calculations predict that the Weyl points in $Mo_xW_{1-x}Te_2$ are above the Fermi level [22, 24, 25]. This makes it challenging to access the Weyl semimetal state with conventional angle-resolved photoemission spectroscopy (ARPES). Recently, we have demonstrated that we can access the unoccupied band structure of $Mo_xW_{1-x}Te_2$ by pump-probe ARPES to the energy range necessary to study the Weyl points and Fermi arcs [41]. At the same time, despite the promise of $Mo_xW_{1-x}Te_2$ for transport, if the Weyl points

are far from the Fermi level, then the novel phenomena associated with the emergent Weyl fermions and violation of Lorentz invariance will not be relevant to the material's transport properties.

Here we report the discovery of a Weyl semimetal in $Mo_xW_{1-x}Te_2$ at doping $x = 25\%$. We use pump-probe ARPES to study the band structure above the Fermi level and we directly observe two kinks in a surface state band. We interpret the kinks as corresponding to the end points of a topological Fermi arc surface state. We apply the bulk-boundary correspondance and argue that since the surface state band structure includes a topological Fermi arc, $Mo_xW_{1-x}Te_2$ is a Weyl semimetal [42]. The end points of the Fermi arc also allow us to fix the energy and momentum locations of the Weyl points. We find excellent agreement with our *ab initio* calculation. However, crucially, we find that certain Weyl points have lower binding energy than expected from calculation and, in fact, are located very close to the Fermi level. This unexpected result suggests that our $Mo_{0.25}W_{0.75}Te_2$ samples may be useful to study the unusual transport phenomena of Weyl semimetals and, in particular, those particularly exotic phenomena arising from strongly Lorentz-violating Weyl fermions. Our work also sets the stage for the first tunable Weyl semimetal. Our discovery of a Weyl semimetal in $Mo_xW_{1-x}Te_2$ provides the first Weyl semimetal outside the TaAs family, as well as a Weyl semimetal which may be tunable and easily accessible in transport studies. Taken together with calculation, our experimental results further show that we have realized the first Weyl semimetal with Type II, or strongly Lorentz-violating, emergent Weyl fermions.

RESULTS

Overview of the crystal and electronic structure

We first provide a brief background of $Mo_xW_{1-x}Te_2$ and study the band structure below the Fermi level. WTe_2 crystallizes in an orthorhombic Bravais lattice, space group $Pmn2_1$ (#31), lattice constants $a = 6.282$Å, $b = 3.496$Å, and $c = 14.07$Å, as shown in Fig. 1a [43]. Crucially, the crystal has no inversion symmetry, a requirement for a Weyl semimetal [12]. The crystals we study are flat, shiny, layered and beautiful, see Fig. 1b. The natural cleaving plane is (001), with surface and bulk Brillouin zones as shown in Fig. 1c. We first

consider the overall band structure of WTe_2. There are two bands, one electron and one hole pocket, near the Fermi level, both very near the Γ point of the bulk Brillouin zone, along the $\Gamma - Y$ line. Although the bands approach each other and Weyl points might be expected to arise where the bands cross, it is now understood that WTe_2 is in fact very close to a phase transition between a Weyl semimetal phase and a trivial phase, so that the electronic structure of WTe_2 is too fragile to make it a compelling candidate for a Weyl semimetal [22]. Next, we interpolate between *ab initio* Wannier function-based tight-binding models for WTe_2 and $MoTe_2$ to study $Mo_xW_{1-x}Te_2$ at arbitrary x [22]. For a wide range of x, we find a robust Weyl semimetal phase [22]. In Fig. 1e,f, we show where the Weyl points sit in the Brillouin zone. They are all located close to Γ in the $k_z = 0$ momentum plane. There are two sets of Weyl points, W_1 at binding energies $E_B = -0.045$ eV and W_2 at $E_B = -0.066$ eV, all above the Fermi level E_F. In addition, the Weyl points are almost aligned at the same $k_y = \pm k_W$, although this positioning is not known to be in any way symmetry-protected. We also note that the Weyl cones are all tilted over, corresponding to strongly Lorentz-violating or Type II Weyl fermions, see Fig. 1g [23]. Next, we study a Fermi surface of $Mo_xW_{1-x}Te_2$ at $x = 45\%$ using incident light with photon energy $h\nu = 5.92$ eV, shown in Fig. 1h. We observe two pockets, a palmier-shaped pocket closer to the $\bar{\Gamma}$ point of the surface Brillouin zone and an almond-shaped pocket sitting next to the palmier pocket, further from $\bar{\Gamma}$. The palmier pocket is a hole pocket, while the almond pocket is an electron pocket [41]. We note that we see an excellent agreement between our results and an *ab initio* calculation of $Mo_xW_{1-x}Te_2$ for $x = 40\%$, shown in Fig. 1i. At the same time, we point out that the electron pocket of the Weyl points is nearly absent in this ARPES spectrum, possibly due to low photoemission cross section at the photon energy used [22, 41]. However, as we will see below, we do observe this electron pocket clearly in our pump-probe ARPES measurements, carried out at a slightly different photon energy, $h\nu = 5.92$ eV. Based on our calculations and preliminary ARPES results, we expect that the Weyl points sit above the Fermi level, where the palmier and almond pockets approach each other. We also present an E_B-k_x spectrum in Fig. 1j where we see how the plamier and almond pockets nest into each other. We expect the two pockets to chase each other as they disperse above E_F, giving rise to Weyl points, see Fig. 1k.

Unoccupied band structure of $Mo_xW_{1-x}Te_2$

Next, we show that pump-probe ARPES at probe photon energy $h\nu = 5.92$ eV gives us access to the bulk and surface bands participating in the Weyl semimetal state in $Mo_{0.25}W_{0.75}Te_2$, both below and above E_F. In Fig. 2a-c, we present three successive ARPES spectra of $Mo_{0.25}W_{0.75}Te_2$ at fixed k_y near the predicted position of the Weyl points. We observe a beautiful sharp band near E_F, whose sharpness suggests that it's a surface band, and broad continua above and below the Fermi level, whose broad character suggests that they are bulk valence and conduction bands. In Fig. 2d-f, we show the same cuts, with guides to the eye to mark the bulk valence and conduction band continua. We also find that we can track the evolution of the bulk valence and conduction bands clearly in our data with k_y. Specifically, we see that both the bulk valence and conduction bands disperse toward negative binding energies as we sweep k_y closer to $\bar{\Gamma}$. At the same time, we note that the bulk valence band near $\bar{\Gamma}$ is only visible near $k_x \sim 0$ and drops sharply in photoemission cross-section away from $k_x \sim 0$. In Fig. 2g,h we present a comparison of our ARPES data with an *ab initio* calculation of $Mo_{0.25}W_{0.75}Te_2$ [22]. We also mark the location of the three successive spectra on a Fermi surface in Fig. 2i. We include as well the approximate locations of the Weyl points, as expected from calculation. We find excellent correspondence between both bulk and surface states. We add that there is an additional surface state detaching from the bulk conduction band well above the Fermi level and that we can also directly observe this additional surface state both in our ARPES spectra and in calculation. Our pump-probe ARPES results clearly show both the bulk and surface band structure of $Mo_{0.25}W_{0.75}Te_2$, both below and above E_F, and with an excellent correspondence with calculation.

Observation of a topological Fermi arc above the Fermi level

Now we show that we observe signatures of a Fermi arc in $Mo_{0.25}W_{0.75}Te_2$. We consider the cut shown in Fig. 3a, repeated from Fig. 2b, and we study the surface state. We observe two kinks in each branch, at $E_B \sim -0.005$ eV and $E_B \sim -0.05$ eV. This kink is a smoking-gun signature of a Weyl point [42]. We claim that each kink corresponds to a Weyl point and that the surface state passing through them includes a topological Fermi arc. To

show these kinks more clearly, in Fig. 3b, we show a second derivative plot of the spectrum in Fig. 3a. In Fig. 3c we also present a cartoon of the kink in our data, with the positions of the W_1 and W_2 Weyl points marked. Again, note that although the W_1 and W_2 are not located strictly at the same k_y, we expect the k_y separation to be on the order of 10^{-4}Å^{-1} from calculation, so that we can consider them to lie at the same k_y within experimental resolution. We emphasize that from our pump-probe ARPES spectrum, we can directly read off that the energy separation of the Weyl points is ~ 0.05 eV and that the W_1 are located at ~ -0.005 eV. We also present a quantitative analysis of our data, showing a kink. To do this, we fit the surface state momentum distribution curves (MDCs) to a Lorentzian distribution and we plot the train of peaks corresponding to the surface state band. We note that we simultaneously fit the topological surface state, the bulk valence and conduction states and the trivial surface state above the conduction band. In Fig. 3d we plot the resulting band dispersions in white and observe an excellent fit to our spectrum. Next, we define a kink as a failure of the train of Lorentzian maxima to fit to a quadratic band. In particular, over a small energy and momentum window, any band should be well-characterized by a quadratic fit, so the failure of such a fit in a narrow energy window implies a kink. After fitting the topological surface state to a quadratic polynomial we find two mismatched regions, marked in Fig. 3e, demonstrating two kinks. For comparison, we plot the energy positions of the W_1 and W_2 as read off directly from Fig. 3a. We find an excellent agreement between the qualitative and quantitative analysis, although we note that the fit claims that the W_2 kink is lower in energy. To illustrate the success of the Lorentzian fit, in Figs. 3f,g we present two representative MDCs at energies indicated by the green arrows. We see that the Lorentzian distributions provide a good fit and take into account all bands observed in our spectra. The raw data, the second derivative plots and the Lorentzian fitting all show two kinks, providing a strong signature of Fermi arcs.

To show that we have observed a topological Fermi arc, we compare our experimental observation of two surface state kinks with a numerical calculation of $Mo_{0.25}W_{0.75}Te_2$. In Fig. 4a,b, we mark the energies of the Weyl points as well as the band minimum of the surface state in our ARPES spectrum and in calculation. We see that the energy difference between the Weyl points is ~ 0.02 eV in calculation but ~ 0.05 eV in experiment. Moreover, the band minimum E_{min} is at $\sim E_{\text{F}}$ in calculation, but at $E_{\text{B}} \sim 0.06$ eV in experiment. The difference in E_{min} suggests either that our sample is electron-doped or that the k_y position

of the Weyl points differs in experiment and theory. Next, crucially, we observe that, in disagreement with calculation, the W_1 are located only ~ 0.005 eV above E_{F}. This suggests that the Weyl points and Fermi arcs in our $Mo_{0.25}W_{0.75}Te_2$ samples may be accessible in transport. This result is particularly relevent because $MoTe_2$, WTe_2 and other transition metal dichalcogenides are already under study as platforms for novel electronics [26–30]. Since the Weyl points of $Mo_xW_{1-x}Te_2$ may be at the Fermi level, it is possible that transport measurements may detect a signature of the strongly Lorentz-violating Weyl fermions or other unusual transport phenomena associated with Weyl semimetals in $Mo_xW_{1-x}Te_2$. We summarize our results in Fig. 4c. We directly observe, above the Fermi level, a surface state with two kinks (shown in red). By comparing our results with *ab initio* calculation, we confirm that the kinks correspond to Weyl points. Furthermore, the excellent agreement of our experimental results with calculation shows that we have realized the first Type II Weyl semimetal.

Limits on directly observing Type II Weyl cones

So far we have studied the surface states of $Mo_xW_{1-x}Te_2$ and we have argued that $Mo_xW_{1-x}Te_2$ is a Weyl semimetal because we observe a topological Fermi arc surface state. However, topological Fermi arcs cannot strictly distinguish between bulk Weyl cones that are of Type I or Type II. While the excellent agreement with calculation suggests that $Mo_xW_{1-x}Te_2$ is a Type II Weyl semimetal, we might ask if we can directly observe a Type II Weyl cone in $Mo_xW_{1-x}Te_2$ by ARPES. This corresponds to observing the two branches of the bulk Weyl cone, as indicated by the purple dotted circles in Fig. 4c. We reiterate that one crucial obstacle in observing a Type II Weyl cone is that all the recent calculations on WTe_2, $Mo_xW_{1-x}Te_2$ and $MoTe_2$ predict that all Weyl points are above the Fermi level [22–25]. As we have seen, using pump-probe ARPES, we are able to measure the unoccupied band structure and show a Fermi arc. However, in our pump-probe ARPES measurements, we find that the photoemission cross-section of the bulk bands is too weak near the Weyl points. At the same time, our calculations suggest that for a reasonable quasiparticle lifetime and spectral linewidth, the broadening of bands will make it difficult to resolve the two branches of the Weyl cone. We conclude that it is challenging to directly access the Type II Weyl cones in $Mo_xW_{1-x}Te_2$.

Considerations regarding trivial surface states

One obvious concern with our experimental result is that we observe two kinks in the surface state, but we expect a disjoint segment based on topological theory. In particular, all calculations show that all Weyl points in $Mo_xW_{1-x}Te_2$ have chiral charge ± 1 [22–25]. However, our observation of a kink suggests that there are two Fermi arcs connecting to the same Weyl point, which requires a chiral charge of ± 2. To resolve this contradiction, we study the calculation of the surface state near the Weyl points, shown in Fig. 4g. We observe, as expected, a Fermi arc (red arrow) connecting the Weyl points. However, at the same time, we see that trivial surface states (yellow arrows) from above and below the band crossing merge with the bulk bands in the vicinity of the Weyl points. As a result, there is no disjoint arc but rather a large, broadband surface state with a ripple arising from the Weyl points. We can imagine that this broadband surface state exists even in the trivial phase. Then, when the bulk bands cross and give rise to Weyl points, a Fermi arc is pulled out from this broadband surface state. At the same time, the remainder of the broadband surface state survives as a trivial surface state. In this way, the Fermi arc is not disjoint but shows up as a ripple. We observe precisely this ripple in our ARPES spectra of $Mo_{0.25}W_{0.75}Te_2$.

As a further check of our analysis, we perform a Lorentzian fit of an ARPES spectrum at k_y shifted away from the Weyl points, shown in Fig. 4d, the same cut as Fig. 2c. We show the Lorentzian fit in Fig. 4e and a quadratic fit to the train of peaks in Fig. 2f. In sharp contrast to the result for $k_y \sim k_W$, there is no ripple in the spectrum and the quadratic provides an excellent fit. This result is again consistent with our expectation that we should observe a ripple only at k_y near the Weyl points. Our results also set the stage for the realization of the first tunable Weyl semimetal in $Mo_xW_{1-x}Te_2$. As we vary the composition, we expect to tune the relative separation of the Weyl points and E_F. In Fig. 4h-k, we present a series of calculations of $Mo_xW_{1-x}Te_2$ for $x = 10\%$, 25%, 40% and 100%. We see that the separation of the Weyl points increases with x and that the W_1 approach E_F for larger x. We propose that a systematic composition dependence can demonstrate the first tunable Weyl semimetal in $Mo_xW_{1-x}Te_2$.

DISCUSSION

We have demonstrated a Weyl semimetal in $Mo_xW_{1-x}Te_2$ by directly observing kinks and a Fermi arc in the surface state band structure. Taken together with calculation, our experimental data show that we have realized the first Type II Weyl semimetal, with strongly Lorentz-violating Weyl fermions. We point out that in contrast to concurrent works on the Weyl semimetal state in $MoTe_2$ [44–52], we directly access the unoccupied band structure of $Mo_xW_{1-x}Te_2$ and directly observe a Weyl semimetal with minimal reliance on calculation. In particular, our observation of a surface state kink at a generic point in the surface Brillouin zone requires that the system be a Weyl semimetal [42]. The excellent agreement with calculation serves as an additional, independent check of our experimental results. We also reiterate that unlike $MoTe_2$, $Mo_xW_{1-x}Te_2$ opens the way to the realization of the first tunable Weyl semimetal. Lastly, we note that $MoTe_2$ is complicated because it is near a critical point for a topological phase transition. Indeed, one recent theoretical work [24] shows that $MoTe_2$ has four Weyl points, while another [25] finds eight Weyl points. Indeed, this is similar to the case of WTe_2, which is near the critical point for a transition between eight Weyl points and zero Weyl points. By contrast, $Mo_xW_{1-x}Te_2$ sits well within the eight Weyl point phase for most x, as confirmed explicity here and in Ref. [22]. The stability of the topological phase of $Mo_xW_{1-x}Te_2$ simplifies the interpretation of our data. By directly demonstrating a Weyl semimetal in $Mo_xW_{1-x}Te_2$, we provide not only the first Weyl semimetal beyond the TaAs family, but the first Type II Weyl semimetal, as well as a Weyl semimetal which may be tunable and which may be more accessible for transport and optics studies of the fascinating phenomena arising from emergent Weyl fermions in a crystal.

METHODS

Pump-probe ARPES

Pump-probe ARPES measurements were carried out using a hemispherical Scienta R4000 analyzer and a mode-locked Ti:Sapphire laser system that delivered 1.48 eV pump and 5.92 eV probe pulses at a repetition rate of 250 kHz [53]. The time and energy resolution were 300 fs and 15 meV, respectively. The spot diameters of the pump and probe lasers at the sample were 250 μm and 85 μm, respectively. Measurements were carried out at pressures

$< 5 \times 10^{-11}$ Torr and temperatures ~ 8 K.

Sample growth

Single crystals of $Mo_xW_{1-x}Te_2$ were grown using a chemical vapor transport (CVT) technique with iodine as the transport agent. Stoichiometric Mo, W and Te powders were ground together and loaded into a quartz tube with a small amount of I. The tube was sealed under vacuum and placed in a two-zone furnace. The hot zone was maintained at 1050°C for 2 weeks and the cold zone was maintained at 950°C.The dopant distribution is not uniform particularly near the crystal surface. The composition of the selected sample was determined by an energy dispersive spectroscopy (EDS) measurement with a scanning electron microscope (SEM).

***Ab initio* calculations**

The *ab initio* calculations were based on the generalized gradient approximation (GGA) [54] used the full-potential projected augmented wave method [55, 56] as implemented in the VASP package [57]. Experimental lattice constants were used for both WTe_2 [58] and $MoTe_2$. A $15 \times 11 \times 7$ Monkhorst-Pack k-point mesh was used in the computations. The spin-orbit coupling effects were included in calculations. To calculate the bulk and surface electronic structures, we constructed first-principles tight-binding model Hamilton by projecting onto the Wannier orbitals [59–61], which use the VASP2WANNIER90 interface [62]. We used W d orbitals, Mo d orbitals, and Te p orbitals to construct Wannier functions and without perform the procedure for maximizing localization. The electronic structure of the $Mo_xW_{1-x}Te_2$ samples with finite doping was calculated by a linear interpolation of tight-binding model matrix elements of WTe_2 and $MoTe_2$. The surface states were calculated from the surface Green's function of the semi-infinite system [63, 64].

Data availability

The data relevant to the findings of this study are available from the corresponding authors upon reasonable request.

ACKNOWLEDGEMENTS

I.B. thanks Yun Wu, Daixiang Mou, Lunan Huang and Adam Kaminski for collaboration on the conventional laser ARPES measurements and insightful discussions on $Mo_xW_{1-x}Te_2$ and $MoTe_2$. I.B. acknowledges the support of the US National Science Foundation GRFP. Work at Princeton University is supported by the Emergent Phenomena in Quantum Systems (EPiQS) Initiative of the Gordon and Betty Moore Foundation under Grant No. GBMF4547 (M.Z.H.) and by the National Science Foundation, Division of Materials Research, under Grants No. NSF-DMR-1507585 and No. NSF-DMR-1006492. Y.I. is supported by the Japan Society for the Promotion of Science, KAKENHI 26800165. T.-R.C. and H.-T.J. were supported by the National Science Council, Taiwan. H.-T.J. also thanks the National Center for High-Performance Computing, Computer and Information Network Center National Taiwan University, and National Center for Theoretical Sciences, Taiwan, for technical support. M.N. is supported by start-up funds from the University of Central Florida. X.C.P., Y.S., H.J.B., G.H.W and F.Q.S. thank the National Key Projects for Basic Research of China (Grant Nos. 2013CB922100, 2011CB922103), the National Natural Science Foundation of China (Grant Nos. 91421109, 11522432, and 21571097) and the NSF of Jiangsu province (No. BK20130054). This work is also financially supported by the Singapore National Research Foundation under NRF Award No. NRF-NRFF2013-03 (H.L.); NRF Research Fellowship (NRF-NRFF2011-02) and the NRF Medium-sized Centre program (G.E.); and NRF RF Award No. NRF-RF2013-08, the start-up funding from Nanyang Technological University (M4081137.070) (Z.L.).

AUTHOR CONTRIBUTIONS

Pump-probe ARPES measurements were carried out by I. B. and D. S. S. with assistance from S.-Y. X., N. A., G. B. and M. N. The pump-probe ARPES system was maintained, calibrated and optimized by Y. I. with assistance from T. K. and under the direction of S. S. Samples were grown by X. P., P. Y., Z. L. and F. S. with assistance from Y. S., H. B. and G. W. G. C., T.-R. C., S.-M. H., C.-C. L., H.-T. J. and H. L. carried out numerical calculations with experimental data on lattice constants provided by S. L. and G. E. The manuscript was written primarily by I. B., D. S. S., Y. I. and S.-Y. X., with valuable insights

and comments from all authors. M. Z. H. provided overall direction, planning and guidance for the project.

COMPETING INTERESTS

The authors declare that they have no competing interests.

† Electronic address: z.liu@ntu.edu.sg

‡ Electronic address: songfengqi@nju.edu.cn

§ Electronic address: mzhasan@princeton.edu

[1] Xu, S.-Y. *et al.* Discovery of a Weyl fermion semimetal and topological Fermi arcs. *Science* **349**, 613-617 (2015).

[2] Lu, L. *et al.* Experimental observation of Weyl points. *Science* **349**, 622-624 (2015).

[3] Lv, B. Q. *et al.* Experimental discovery of Weyl semimetal TaAs. *Phys. Rev. X* **5**, 031013 (2015).

[4] Huang, S.-M. *et al.* A Weyl Fermion semimetal with surface Fermi arcs in the transition metal monopnictide TaAs class. *Nat. Commun.* **6**, 7373 (2015).

[5] Weng, H., Fang, C., Fang, Z., Bernevig, B. A. & Dai, X. Weyl semimetal phase in noncentrosymmetric transition-metal monophosphides. *Phys. Rev. X* **5**, 011029 (2015).

[6] Weyl, H. Elektron und gravitation. *Z. Phys.* **56**, 330-352 (1929).

[7] Peskin, M. & Schroeder, D. *An Introduction to Quantum Field Theory* (Perseus Books Publishing, 1995).

[8] Herring, C. Accidental degeneracy in the energy bands of crystals. *Phys. Rev.* **52**, 365-373 (1937).

[9] Abrikosov, A. A. & Beneslavskii, S. D. Some properties of gapless semiconductors of the second kind. *J. Low Temp. Phys.* **5**, 141-154 (1971).

[10] Nielsen, H. B. & Ninomiya, M. The Adler-Bell-Jackiw anomaly and Weyl fermions in a crystal. *Phys. Lett. B* **130**, 389-396 (1983).

[11] Volovik, G. E. *The Universe in a Helium Droplet* (Oxford University Press, 2003).

[12] Murakami, S. Phase transition between the quantum spin Hall and insulator phases in 3D:

emergence of a topological gapless phase. *New J. Phys.* **9**, 356 (2007).

[13] Burkov, A. A. & Balents, L. Weyl semimetal in a topological insulator multilayer. *Phys. Rev. Lett.* **107**, 127205 (2011).

[14] Wan, X., Turner, A. M., Vishwanath, A. & Savrasov, S. Y. Topological semimetal and Fermi-arc surface states in the electronic structure of pyrochlore iridates. *Phys. Rev. B* **83**, 205101 (2011).

[15] Turner, A. & Vishwanath, A. Beyond band insulators: topology of semi-metals and interacting phases. Preprint at https://arxiv.org/abs/1301.0330 (2013).

[16] Parameswaran, S. A., Grover, T., Abanin, D. A., Pesin, D. A. & Vishwanath, A. Probing the Chiral Anomaly with Nonlocal Transport in Three-Dimensional Topological Semimetals. *Phys. Rev. X* **4**, 031035 (2014).

[17] Hosur, P. & Qi, X. Recent developments in transport phenomena in Weyl semimetals. *Comp. Rend. Phy.* **14**, 857-870 (2013).

[18] Potter, A. C., Kimchi, I. & Vishwanath, A. Quantum oscillations from surface Fermi arcs in Weyl and Dirac semimetals. *Nat. Commun.* **5**, 5161 (2014).

[19] Zhang, C. *et al.* Signatures of the Adler-Bell-Jackiw chiral anomaly in a Weyl semimetal. *Nat. Commun.* **7**, 10735 (2016).

[20] Huang, X. *et al.* Observation of the Chiral-Anomaly-Induced Negative Magnetoresistance in 3D Weyl Semimetal TaAs. *Phys. Rev. X* **5**, 031023 (2015).

[21] Shekhar, C. *et al.* Extremely large magnetoresistance and ultrahigh mobility in the topological Weyl semimetal candidate NbP. *Nat. Phys.* **11**, 645-649 (2015).

[22] Chang, T.-R. *et al.* Prediction of an arc-tunable Weyl Fermion metallic state in $Mo_xW_{1-x}Te_2$. *Nat. Commun.* **7**, 10639 (2016).

[23] Soluyanov, A. *et al.* Type II Weyl semimetals. *Nature* **527**, 495-498 (2015).

[24] Wang, Z. J. *et al.* $MoTe_2$: A Type-II Weyl Topological Metal. *Phys. Rev. Lett.* **117**, 056805 (2016).

[25] Sun, Y., Wu, S.-C., Ali, M. N., Felser, C. & Yan, B. Prediction of Weyl semimetal in orthorhombic $MoTe_2$. *Phys. Rev. B* **92**, 161107 (2015).

[26] Mak, K. F. & Shan, J. Photonics and optoelectronics of 2D semiconductor transition metal dichalcogenides. *Nat. Photon.* **10**, 216-226 (2016).

[27] Qian, X. F., Liu, J., Fu, L. & Li, J. Quantum spin Hall effect in two-dimensional transition

metal dichalcogenides. *Science* **346**, 1344-1347 (2014).

[28] Cho, S. *et al.* Phase patterning for ohmic homojunction contact in $MoTe_2$. *Science* **349**, 625-628 (2015).

[29] Mak, K. F., Lee, C., Hone, J., Shan, J. & Heinz, T. F. Atomically Thin MoS_2: A New Direct-Gap Semiconductor. *Phys. Rev. Lett.* **105**, 136805 (2010).

[30] Cao, T. *et al.* Valley-selective circular dichroism of monolayer molybdenum disulphide. *Nat. Commun.* **3**, 887 (2012).

[31] Grushin, A. G. Consequences of a condensed matter realization of Lorentz-violating QED in Weyl semi-metals. *Phys. Rev. D* **86**, 045001 (2012).

[32] Bergholtz, E. J., Liu, Z., Trescher, M., Moessner, R. & Udagawa, M. Topology and Interactions in a Frustrated Slab: Tuning from Weyl Semimetals to $C > 1$ Fractional Chern Insulators. *Phys. Rev. Lett.* **114**, 016806 (2015).

[33] Trescher, M., Sbierski, B., Brouwer, P. W. & Bergholtz, E. J. Quantum transport in Dirac materials: Signatures of tilted and anisotropic Dirac and Weyl cones. *Phys. Rev. B* **91**, 115135 (2015).

[34] Beenakker, C. Tipping the Weyl cone. *Journal Club for Condensed Matter Physics*. Posted at http://www.condmatjournalclub.org/?p=2644 (2015).

[35] Chang, G. *et al.* A strongly robust type II Weyl fermion semimetal state in Ta_3S_2. *Sci. Adv.* **2**, e1600295 (2016).

[36] Koepernik, K. *et al.* $TaIrTe_4$: A ternary type-II Weyl semimetal. *Phys. Rev. B* **93**, 201101 (2016).

[37] Autés, G., Gresch, D., Troyer, M., Soluyanov, A. A. & Yazyev O. V. Robust Type-II Weyl Semimetal Phase in Transition Metal Diphosphides XP_2 (X =Mo, W). *Phys. Rev. Lett.* **117**, 066402 (2016).

[38] Xu, S.-Y. *et al.* Discovery of Lorentz-violating Weyl fermion semimetal state in LaAlGe materials. Preprint at https://arxiv.org/abs/1603.07318 (2016).

[39] Zyuzin, A. A. & Tiwari, R. P. Intrinsic anomalous Hall effect in type-II Weyl semimetals. *JETP* **103**, 717-722 (2016).

[40] Isobe, H. & Nagaosa, N. Coulomb interaction effect in tilted Weyl fermion in two dimensions. *Phys. Rev. Lett.* **116**, 116803 (2016).

[41] Belopolski, I. *et al.* Fermi arc electronic structure and Chern numbers in the type-II Weyl

semimetal candidate $Mo_xW_{1-x}Te_2$. *Phys. Rev. B* **94**, 085127 (2016).

[42] Belopolski, I. *et al.* Criteria for Directly Detecting Topological Fermi Arcs in Weyl Semimetals. *Phys. Rev. Lett.* **116**, 066802 (2016).

[43] Brown, B. E. The crystal structures of WTe_2 and high-temperature $MoTe_2$. *Acta. Cryst.* **20** 268-274 (1966).

[44] Huang, L. *et al.* Spectroscopic evidence for type II Weyl semimetallic state in $MoTe_2$. *Nat. Mat.* DOI:10.1038/nmat4685 (2016).

[45] Deng, K. *et al.* Experimental observation of topological Fermi arcs in type-II Weyl semimetal $MoTe_2$. DOI:10.1038/nphys3871 (2016).

[46] Tamai, A. *et al.* Fermi Arcs and Their Topological Character in the Candidate Type-II Weyl Semimetal $MoTe_2$. *Phys. Rev. X* **6**, 031021 (2016).

[47] Wu, Y. *et al.* Observation of Fermi arcs in the type-II Weyl semimetal candidate WTe_2. *Phys. Rev. B* **94**, 121113 (2016).

[48] Bruno, F. Y., *et al.* Observation of large topologically trivial Fermi arcs in the candidate type-II Weyl semimetal WTe_2. *Phys. Rev. B* **94**, 121112 (2016).

[49] Jiang, J. *et al.* Observation of the Type-II Weyl Semimetal Phase in $MoTe_2$. Preprint at https://arxiv.org/abs/1604.00139 (2016).

[50] Liang, A. *et al.* Electronic Evidence for Type II Weyl Semimetal State in $MoTe_2$. Preprint at https://arxiv.org/abs/1604.01706 (2016).

[51] Wang, C. *et al.* Spectroscopic Evidence of Type II Weyl Semimetal State in WTe_2. Preprint at https://arxiv.org/abs/1604.04218 (2016).

[52] Xu, N. *et al.* Discovery of Weyl semimetal state violating Lorentz invariance in $MoTe_2$. Preprint at https://arxiv.org/abs/1604.02116 (2016).

[53] Ishida, Y. *et al.* Time-resolved photoemission apparatus achieving sub-20-meV energy resolution and high stability. *Rev. Sci. Instr.* **85**, 123904 (2014).

[54] Perdew, J. P., Burke, K. & Ernzerhof, M. Generalized gradient approximation made simple. *Phys. Rev. Lett.* **77**, 3865 (1996).

[55] Blöchl, P. E. Projector augmented-wave method. *Phys. Rev. B.* **50**, 17953 (1994).

[56] Kresse, G. & Joubert, J. From ultrasoft pseudopotentials to the projector augmented-wave method. *Phys. Rev. B.* **59**, 1758 (1999).

[57] Kresse, G. & Furthmüller, J. Efficiency of *ab initio* total energy calculations for metals and

semiconductors using a plane-wave basis set. *Comput. Mater. Sci.* **6**, 15-50 (1996).

[58] Mar, A., Jobic, S. & Ibers, J. A. Metal-metal vs. tellurium-tellurium bonding in WTe_2 and its ternary variants $TaIrTe_4$ and $NbIrTe_4$. *J. Am. Chem. Soc.* **114**, 8963 -8971 (1992).

[59] Marzari, N. & Vanderbilt, D. Maximally localized generalized Wannier functions for composite energy bands. *Phys. Rev. B* **56**, 12847 (1997).

[60] Souza, I., Marzari, N. & Vanderbilt, D. Maximally localized Wannier functions for entangled energy bands. *Phys. Rev. B* **65**, 035109 (2001).

[61] Mostofi, A. A., Yates, J. R., Lee, Y.-S., Souza, I., Vanderbilt, D. & Marzari, N. Wannier90: a tool for obtaining maximally-localized Wannier functions. *Comp. Phys. Commun.* **178**, 685-699 (2008).

[62] Franchini, C. *et al.* Maximally localized Wannier functions in $LaMnO_3$ within PBE+U, hybrid functionals and partially self-consistent GW: an efficient route to construct *ab initio* tight-binding parameters for e_g perovskites. *J. Phys. Cond. Mat.* **24**, 235602 (2012).

[63] Xia, Y. *et al.* Observation of a large-gap topological-insulator class with a single Dirac cone on the surface. *Nat. Phys.* **5**, 398-402 (2009).

[64] Zhang, H., Liu, C.-X., Qi X.-L., Dai, X., Fang, Z. & Zhang, S.-C. Topological insulators in Bi_2Se_3, Bi_2Te_3 and Sb_2Te_3 with a single Dirac cone on the surface. *Nat. Phys.* **5**, 438-442 (2009).

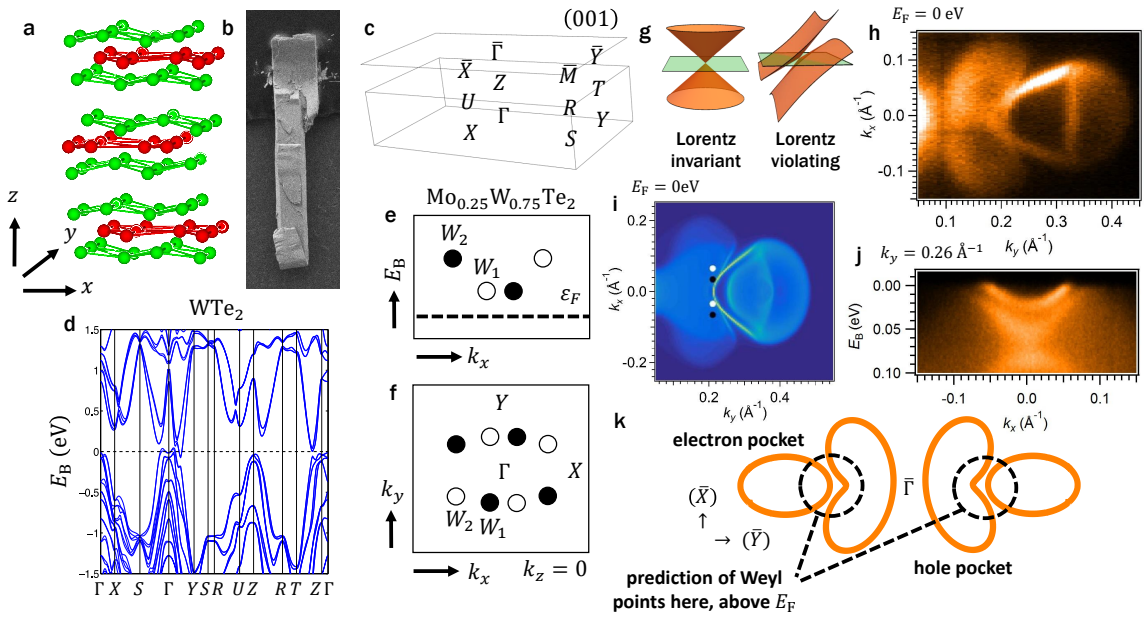
a
b
c
(001)
g
h
E_F = 0 eV
Lorentz invariant
Lorentz violating
z
y
x
WTe2
d
E_B (eV)
Γ X S Γ YSR UZ RT ZΓ
$Mo_{0.25}W_{0.75}Te_2$
e
W_2
W_1
ε_F
E_B
k_x
f
Y
Γ
X
k_y
W_2 W_1
k_z = 0
i
E_F = 0eV
k_x (Å^{-1})
k_y (Å^{-1})
j
k_y = 0.26 Å^{-1}
k_y (Å^{-1})
E_B (eV)
k
electron pocket
$(\bar{X})$
$(\bar{Y})$
$\bar{\Gamma}$
hole pocket
prediction of Weyl points here, above E_F

FIG. 1: **Overview of $Mo_xW_{1-x}Te_2$. a,** The crystal structure of the system is layered, with each monolayer consisting of two Te layers (green) and one W/Mo layer (red). **b,** A wonderful scanning electron microscope (SEM) image of a typical single crystal of $Mo_xW_{1-x}Te_2$, $x = 45\%$. The layered structure is visible in the small corrugations and breaks in the layers. **c,** Bulk and (001) surface Brillouin zone, with high-symmetry points marked. **d,** Bulk band structure of WTe_2 along high-symmetry lines. There are two relevant bands near the Fermi level, an electron band and a hole band, both near the Γ point and along the $\Gamma - Y$ line, which approach each other near the Fermi level. **e, f,** Upon doping by Mo, $Mo_xW_{1-x}Te_2$ enters a robust Weyl semimetal phase [22]. Schematic of the positions of the Weyl points in the bulk Brillouin zone. The opposite chiralities are indicated by black and white circles. Crucially, all Weyl points are above the Fermi level. **g,** The Weyl cones in $Mo_xW_{1-x}Te_2$ are unusual in that they are all tilted over, associated with strongly Lorentz-violating or Type II Weyl fermions, prohibited in particle physics [23]. **h,** Fermi surface of $Mo_xW_{1-x}Te_2$ at $x = 45\%$ measured by ARPES at $h\nu = 6.36$ eV, showing a hole-like palmier pocket and an electron-like almond pocket [41]. **i,** There is an excellent correspondence between our ARPES data and our calculation. Note that the k_y axis on the Fermi surface from ARPES is set by comparison with calculation. **j,** An E_B-k_x cut showing the palmier and almond pockets below the Fermi level. **k,** In summary, the Fermi surface of $Mo_xW_{1-x}Te_2$ consists of a palmier hole pocket and an almond electron pocket near the $\bar{\Gamma}$ point. The two pockets chase each other as they disperse, eventually intersecting above E_F to give Weyl points.

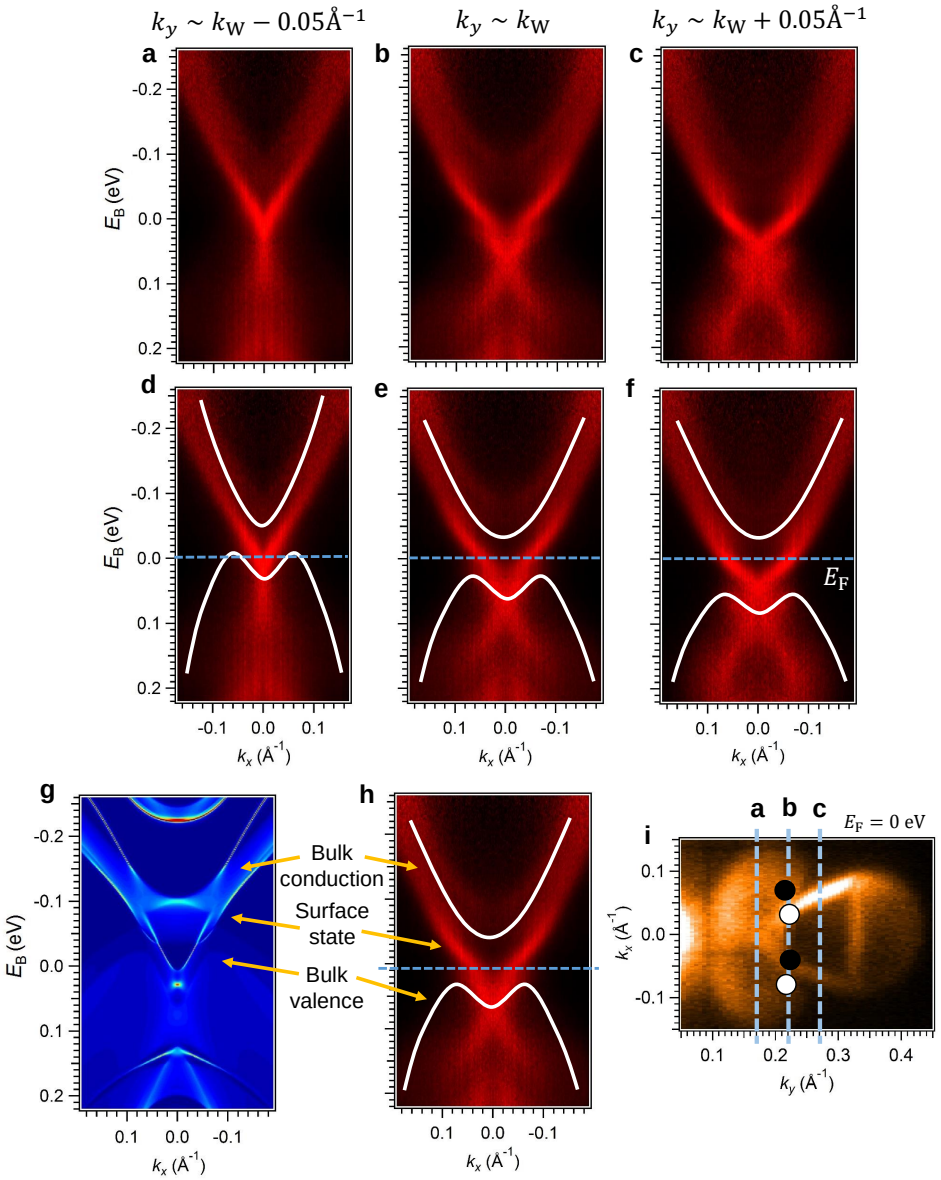
$k_y \sim k_W - 0.05Å^{-1}$
$k_y \sim k_W$
$k_y \sim k_W + 0.05Å^{-1}$
a
b
c
d
e
f
g
h
i
E_B (eV)
k_x (Å^{-1})
E_F
Bulk conduction
Surface state
Bulk valence
$E_F = 0$ eV
k_y (Å^{-1})

FIG. 2: **Dispersion of the unoccupied bulk and surface states of $Mo_{0.25}W_{0.75}Te_2$. a-c,** Three successive ARPES spectra for $Mo_{0.25}W_{0.75}Te_2$ at fixed k_y near the expected position of the Weyl points, k_{Weyl}, using pump-probe ARPES at probe $h\nu = 5.92$ eV. A strong pump response allows us to probe the unoccupied states ~ 0.3 eV above E_F, which is well above the expected E_{W1} and E_{W2}. **d-f,** Same as (a-c), but with the bulk valence and conduction band continuum marked with guides to the eye. We see that we observe all bulk and surface states participating in the Weyl semimetal state. As expected, both the bulk valence and conduction bands move towards more negative binding energies as k_y moves towards $\bar{\Gamma}$. **g, h,** Comparison of our calculations with experimental results for $k_y \sim k_{\mathrm{Weyl}}$. As can be seen from (h), our spectra clearly display all bulk and surface bands of $Mo_{0.25}W_{0.75}Te_2$ relevant for the Weyl semimetal state, both below and above E_F, and with an excellent agreement with the corresponding calculation in panel g. **i,** The locations of the cuts in (a-c).

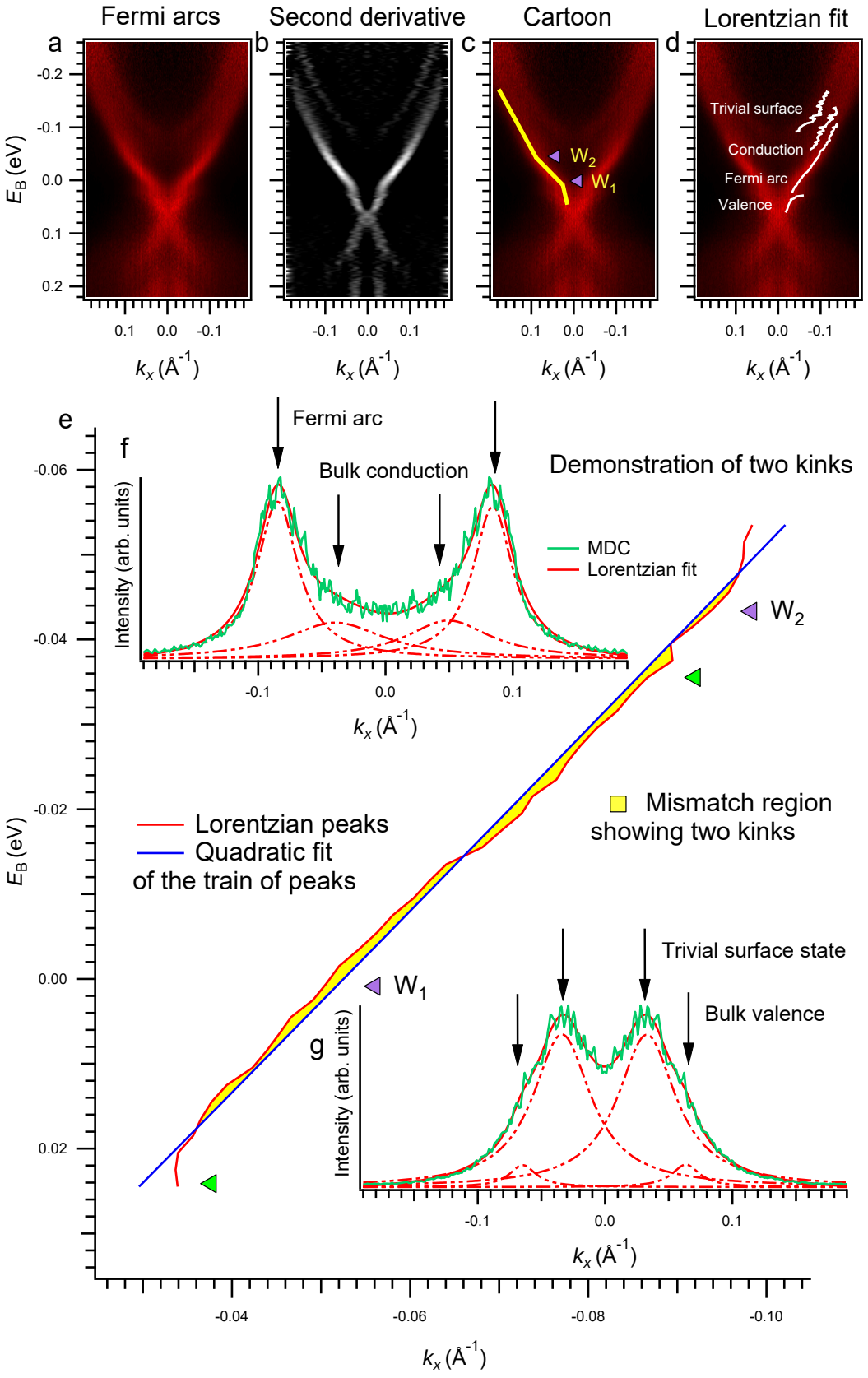
Fermi arcs
Second derivative
Cartoon
Lorentzian fit
a
b
c
d
E_B (eV)
k_x (Å^{-1})
W$_2$
W$_1$
Trivial surface
Conduction
Fermi arc
Valence
e
f
g
Fermi arc
Bulk conduction
Demonstration of two kinks
MDC
Lorentzian fit
Intensity (arb. units)
Lorentzian peaks
Quadratic fit
of the train of peaks
Mismatch region
showing two kinks
Trivial surface state
Bulk valence

FIG. 3: **Direct experimental observation of Fermi arcs in $Mo_{0.25}W_{0.75}Te_2$. a,** To establish the presence of Fermi arcs in $Mo_{0.25}W_{0.75}Te_2$ we focus on spectrum shown in Fig. 2b, with $k_y \sim k_{\mathrm{Weyl}}$. We observe two kinks in the surface state, at $E_B \sim -0.005$ eV and $E_B \sim -0.05$ eV. **b,** The kinks are easier to see in a second-derivative plot of panel a. **c,** Same as panel a, but with a guide to the eye showing the kinks. The Weyl points are at the locations of the kinks. The surface state with the kinks contains a topological Fermi arc. **d,** To further confirm the presence of a kink, we fit Lorentzian distributions to our data. We capture all four bands in the vicinity of the kinks: the bulk conduction and valence states, the topological surface state and an additional trivial surface state merging into the conduction band at more negative E_B. We define a kink as a failure of a quadratic fit to a band. We argue that for a small energy and momentum window, any band should be well-characterized by a quadratic fit and that the failure of such a fit shows a kink. **e,** By matching the train of Lorentzian peaks of the topological surface state (red) to a quadratic fit (blue) we find two mismatched regions (shaded in yellow), showing two kinks. The purple arrows show the location of the Weyl points, taken from panel c, and are consistent with the kinks we observe by fitting. **f, g,** Two characteristic MDCs at energies indicated by the green arrows in panel e. We see that the Lorentzian distributions provide a good fit and capture all bands observed in our spectra.

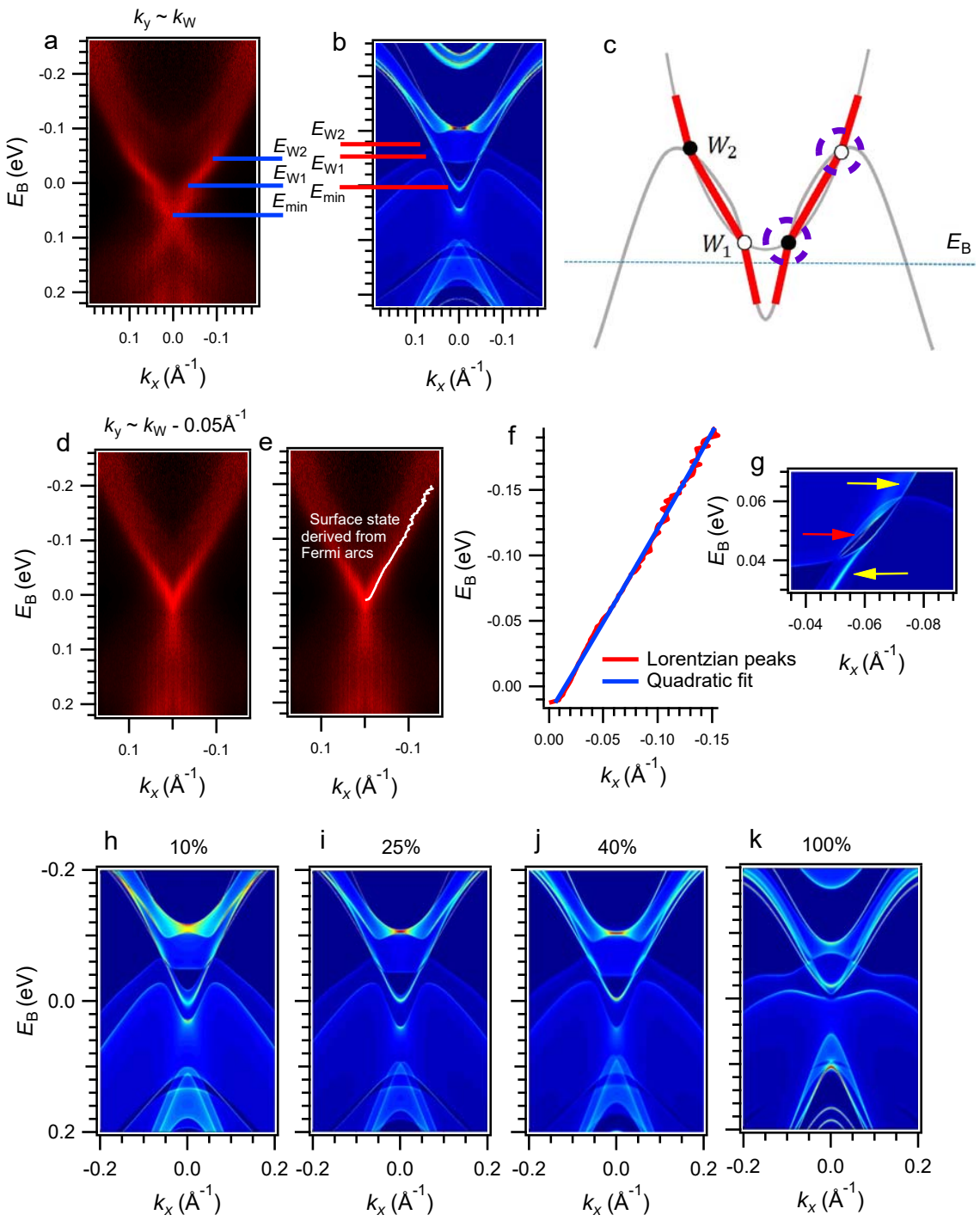
a
$k_y \sim k_W$
E_{W2}
E_{W1}
E_{min}
E_B (eV)
k_x (Å^{-1})
b
c
W_2
W_1
E_B
d
$k_y \sim k_W$ - 0.05Å^{-1}
e
Surface state derived from Fermi arcs
f
Lorentzian peaks
Quadratic fit
g
h
10%
i
25%
j
40%
k
100%

FIG. 4: **Demonstration of a Weyl semimetal in $Mo_xW_{1-x}Te_2$. a,** The same spectrum as Fig. 3a but with the energies ε_{W1}, ε_{W2}, $\varepsilon_{\min}$ marked. **b,** The same energies marked in an *ab initio* calculation of $Mo_{0.25}W_{0.75}Te_2$. We note that this cut is not taken at fixed $k_y \sim k_W$. Instead, we cut along the exact line defined by W_1 and W_2 in the surface Brillouin zone. Since k_y^{W1} is exceedingly close to k_y^{W2}, this cut essentially corresponds to our experimental data. The Weyl points are ~ 0.05 eV separated in energy in our data, compared to ~ 0.02 eV in calculation. In addition, crucially, the W_1 are lower in energy than we expect from calculation and in fact are located only 0.005 eV above E_F. **c,** A cartoon of our interpretation of our experimental results. We observe the surface state (red) with a kink at the locations of the Weyl points (black and white circles). Each surface state consists of a Fermi arc (middle red segment) and two trivial surface states which merge with bulk bands near the location of the Weyl points. We observe certain portions of the bulk bands (gray), but not the bulk Weyl cones, see the Supplementary Information. **d,** The same spectrum as Fig. 2c, at k_y shifted toward $\bar{\Gamma}$. **e, f,** A Lorentzian fit of the surface state and a quadratic fit to the train of peaks, showing no evidence of a kink. This is precisely what we expect from a cut away from the Weyl points. **g,** A close-up of the band inversion, showing a Fermi arc (red arrow) which connects the Weyl points and trivial surface states (yellow arrows) from above and below which merge with the bulk bands in the vicinity of the Weyl points. **h-k,** Composition dependence of $Mo_xW_{1-x}Te_2$ from first principles, showing that the separation of the Weyl points increases with x. Our observation of a Weyl semimetal in $Mo_{0.25}W_{0.75}Te_2$ sets the stage for the first tunable Weyl semimetal in $Mo_xW_{1-x}Te_2$.